Electronic Supplementary Information for

Hydration breaking and chemical ordering in a levitated NaCl solution droplet beyond metastable zone width limit: Evidence for early stage of two-step nucleation

Hyerim Hwang, Yong Chan Cho, Sooheyong Lee, Yun-Hee Lee, Seongheun Kim, Yong-Jae Kim, Wonhyuk Jo, Patrick Duchstein, Dirk Zahn,* and Geun Woo Lee*

*e-mail: gwlee@kriss.re.kr & dirk.zahn@fau.de

S1. Sample levitation- sample preparation, experimental setup of electrostatic levitation

Sample preparation. We prepared an aqueous brine solution by dissolving NaCl (Aldrich, 99%) in deionized water with concentrations ranging from 252 g/L to 288 g/L (NaCl solute in grams/water solvent in liters). The solution was permeated through a syringe filter with a pore size of 220 nm (JET BIOFIL) to eliminate impurities which can act as potential nucleation sites. The filtered NaCl solution is then injected through a syringe. Once the solution droplet is levitated by applying voltage, it starts evaporating under the ambient conditions at temperature of 24 ± 0.5 °C and relative humidity of 46 ± 1%. The solubility limit for NaCl–360 g/L at 25 °C–differs by less than 0.01 % [1].

Electrostatic levitation (ESL). Figure S1 depicts the whole layout of the solution-ESL apparatus in a schematic drawing. As shown in the inset image, the two copper electrodes are parallel and vertically aligned with ~2 cm separation, which gives sufficient space for levitation, in-situ imaging, and scattering measurements. A high-voltage power amplifier (Trek 10/10B) is connected to the top electrode and the bottom one is positively grounded to optic table. A collimated He-Ne laser (1 mW, 632.8 nm) illuminates the droplet to determine position by a position-sensitive detector (PSD) (Hamamatsu Photonics C10443-03). The PSD gives a feedback signal to the power amplifier through a master-control PC with 500 Hz so that the drop is maintained at a desired position for the entire process.

Sample levitation. A solution droplet with a diameter of ~2.5–3 mm is formed from a needle with polytetrafluoroethylene-coated metal tip (Hamilton 8646-01) which is connected to bottom electrode and placed on the central axis of the two electrodes. When electric voltage increases, Coulomb force pulls the positively charged droplet up from on the top of the needle by overcoming the wetting force on the needle and balances with gravitational force at the set-position. Typical voltage that is applied to levitate a droplet ranges from 800 V to 1700 V, depending on its weight. After the sample delivery, the needle is retracted below the bottom electrode. The intensity of the electric voltage is precisely adjusted so as to maintain the levitated droplet at a desired position; the sample position is maintained within ± 20 μm by the position-voltage feedback routine operated with 500 Hz throughout the experiments. The atomic and molecular structures of the levitated solution droplet are measured as a function of concentration by synchrotron X-ray and micro-Raman scatterings, respectively. The detailed description of the ESL is stated elsewhere in Refs.[3,4].

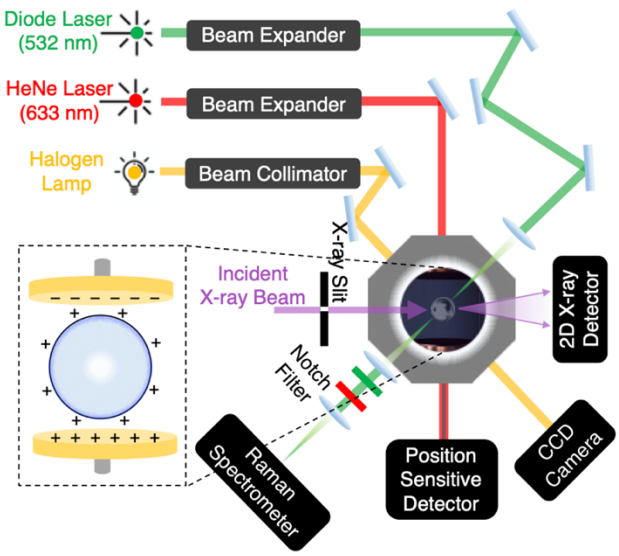

Fig. S1 Schematic of the solution electrostatic levitation apparatus, which enables the structures via Raman spectroscopy and X-ray diffraction. The sample is levitated in an isolated chamber. Inset: schematic drawing of the levitated solution droplet (side view).

S2. Determination of supersaturation

While the evaporation induces the shrinkage of the levitated droplet, the size, shape, and interior of the droplet were continuously monitored via CCD cameras (Lt365R, Lumenera), which was equipped with a 5× magnification zoom lens. The boundary of the droplet image is converted to polar coordinates and fitted by 6th order Legendre polynomial to calculate its volume (V) where $V = 2\pi/3\int_0^{\pi} R(\theta)^3 \sin(\theta) \mathrm{d}(\theta)$. This method has been successfully applied to obtain the volume of the levitated metallic [2] and aqueous solution droplets [3,4]. Since we know the initial amount of solute (NaCl) in the solution and its volume, we can determine the degree of supersaturation.

S3. In-situ synchrotron X-ray diffraction

X-ray scattering experiment was conducted at the sector 1C and 5A beamlines at the Pohang Light Source II. The X-rays from the undulator were monochromatized by cryogenically cooled Si (111) double-crystal monochromator in which the photon energy was set to 21.87 keV. We set-up our ESL apparatus in the sector 1C and 5A beamlines. X-ray detector (Pilatus 300K-W) is placed behind the ESL chamber to collect scattered signals from the levitated solution droplet. Once the levitated droplet approaches to the desired supersaturation, X-ray shutter opens and the scattering data are obtained. Since X-ray beam ionizes air, the surface charge of the levitated droplets and the electrode is disturbed by surrounding air. This causes instability of the sample position, and finally, the droplet falls down. This happens within 1–3 seconds, depending on X-ray beam flux. Therefore, if the scattering signal is not good enough, we carried out the X-ray scattering experiments with multiple trials and with different experimental configurations to achieve wider scattering angle. These trials cause different q ranges in the detection, e.g., 9 $Å^{-1}$ for S = 1.44 and 1.61, and 12 $Å^{-1}$ for other concentrations. Regardless the differences in experiments however, all datasets clearly show the consistent behavior with supersaturation, such as peaks' shape and positions.

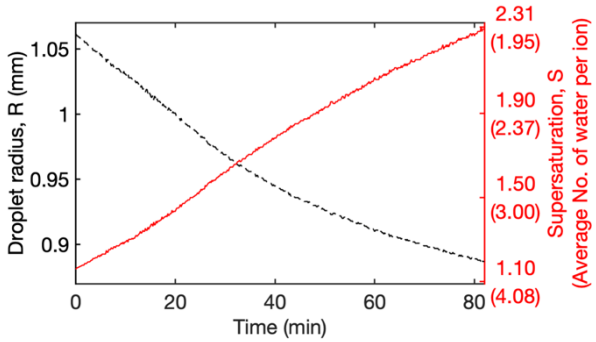

Fig. S2 Temporal changes of the droplet radius (black dashed line) and corresponding supersaturation (red solid line). The average number of water molecules per ion is noted in the round bracket on the right axis.

S4. Molecular dynamics simulations

While the transition path sampling study in Ref.[5] was designed to trigger density fluctuation, unbiased MD simulations were performed for much larger systems and longer relaxation time scales without artificially driving solute dehydration in this study. The MD simulations were carried out with the LAMPPS package using a time-step of 1 fs and the Langevin thermostat-barostat combination [6]. Periodic boundary conditions are applied to mimic bulk solutions. Accordingly, cut-off (1.2 nm) potentials are used in combination with Ewald summation (with a damping constant of 0.5 nm^{-1}). Before sampling, each simulation system was relaxed for 15 ns to ensure convergence of average system energy, volume and the solute distribution. The assessment of pair distribution functions (PDF, g(r)) was performed from 10 ns MD runs after relaxation, which ensures well-converged g(r) profiles sampled with a resolution of 0.01 nm bins. The pair distribution functions compiled from MD trajectories are intrinsically deconvoluted and even further scrutinized by discriminating Na^+ in SSIP in the selective statistics shown in Figure 3.

We note that none of the 1–2 nm scale domains showed immobilization of solute clusters. As none of the ions experiences full dehydration, the domains of large solute density remain liquid and exhibit only short range ordering (see Figure 3(a) for local coordination numbers). Lower solute concentrations (S = 0.77–1.37) were modeled by removing the corresponding number of ions. Each simulation system was relaxed from constant temperature and pressure imposing 300 K and 1 atm, respectively. The molecular interactions were calculated from the SPC/E water model in combination with the NaCl force field of Joung and Cheatham reproduce the solubility concentration in excellent agreement to the experiment [7].

S5. In-situ Raman spectroscopy

The ESL is combined with micro-Raman spectroscope so as to study vibrational mode of water molecules in the levitated NaCl solution. Incident laser beam (532 nm) on the droplet is scattered. The scattered light is delivered to a spectrometer (DONGWOO OPTRON; DM500i) with a diffraction grating (1200 Gr/mm), and then collected on a 2D detector (ANDOR DV401A-Bv) consisting of 1024 ×24 pixels (pixel size of 26 μm^2). In this experiment, a laser power of 1.5 mW was used to minimize the heating of the solution. The exposure time to gather the scattered light is about 40 s.

S6. MD simulation results: pair distribution functions for Na^+-O and Cl^-O

Figure S3 shows the partial g(r) of Na^+-O and Cl^--O. While the data in undersaturation (S = 0.77) is very similar to previous results (Refs. [22,30,31] in the main text), the data at high supersaturation have never been reported. The partial g(r)s of Na^+-O and Cl^--O explains the peaks of experimental g(r) at 2.4 Å and 3.2 Å, but not for 4.0 Å and 4.8 Å.

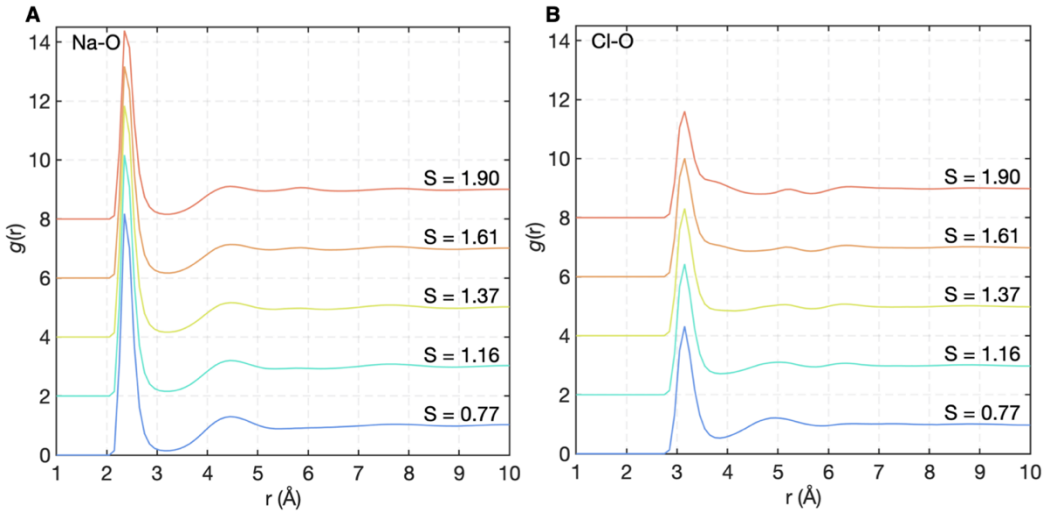

Fig. S3 Partial pair distribution functions for (A) Na^{+}-O and (B) Cl^{-}-O at S = 0.77, 1.16, 1.37, 1.61, and 1.90.

S7. Deconvolution procedure for 5-Gaussian components for Raman spectra

The OH stretching region of the Raman spectra can be deconvoluted into mainly five sub-bands, which are classified as DDAA (double donor–double acceptor), DDA (double donor–single acceptor), DAA (single donor–double acceptor), DA (single donor–single acceptor), and free-OH [8,9]. A useful database for the same or similar experimental conditions were provided, which we refer (Ref.[45] of the main text) as a representative one. The deconvolution parameters are position, amplitude, and width (FWHM) of the peaks, and we used information of the peak position and width of NaCl solution from Refs.[46-48] as a guideline. We begin with a known spectrum of pure water's and convolute it with a Gaussian distribution to obtain the initial parameter input. Then, we deconvolute the Raman spectra of solutions by constraining the solution to lie in a physically meaningful regime at varying concentrations. While we control one parameter during a single fit process, we fix other two parameters; we control width, intensity, and position in sequence.

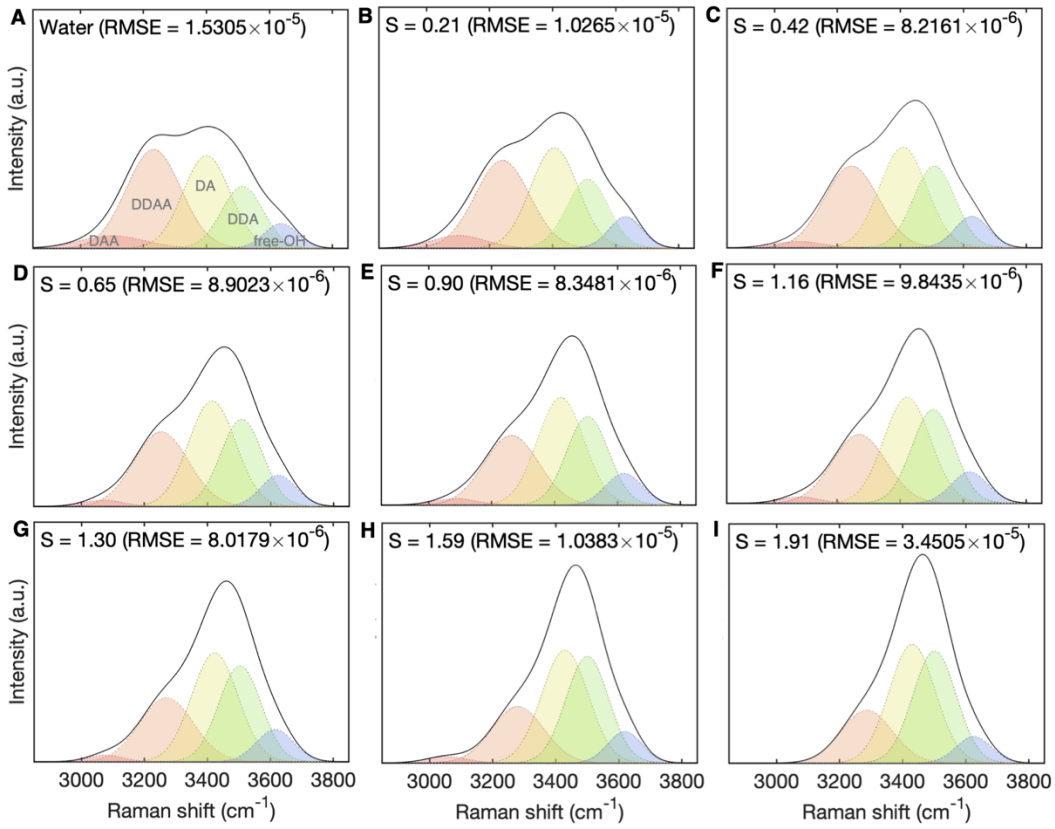

Fig. S4 Raman spectra with 5-Gaussian fitted curves for hydrogen-bonded water configurations (red: DAA, orange: DDAA, yellow: DA, green: DDA, blue: free-OH). (A) water. (B) S = 0.21. (C) S = 0.42. (D) S = 0.65. (E) S = 0.90. (F) S = 1.16. (G) S = 1.30. (H) S = 1.59. (I) S = 1.91. Root mean squared errors (RMSE) are noted for each condition. RMSE = $(\sum(y_e\text{-}y_o)^2/N)^{1/2}$ where y_e, y_o, and N are expected value, observed value, and sample size, respectively.

S8. Fitting procedure of the Raman spectra in the OH stretching region

The measured Raman spectra of the NaCl solution in Figure 4(a) is composed of two contributions, i.e., the O-H stretching modes from water molecules with and without surrounding Na^+ and Cl^- ions. Provided that Na^+ and Cl^- ions are surrounded by an average number of water molecules of 5.5 and 7.5 in their first hydration shell, respectively, and the bulk water is not strongly bound to the first shell, the total Raman spectra (I_{total}) can be deconvoluted into two signals of hydration shell (I_{shell}) and bulk water (I_{water}). This is particularly true in dilute solution (S = 0.1) which comprises completely hydrated ions that are homogeneously suspended, thereby enabling a deduction of I_{shell}, as shown in the inset of Figure 4B. Raman spectra (I_{total}) at different concentrations are fitted with the two curves (I_{water} and I_{shell}) to extract the relative contributions of bulk water α.

S9. Interfacial free energy measurements

Here, we apply the classical nucleation theory (CNT) to estimate the interfacial free energy (IFE), in which the crystal nucleation from solution is critically determined by two terms: surface (σ) and bulk energy ($\Delta\mu$). The CNT is generally described by $\Delta G = 4\pi r^2\sigma - (4\pi r^3/3)\Delta\mu/v_m$, where r is the radius of the nucleus, v_m is the molar volume of the nucleus, and $\Delta\mu = \mu_c - \mu_l$ is the chemical potential difference between the crystal nucleus and liquid. The $\Delta\mu$ can be expressed by $\Delta\mu = k_B T \ln S$ for the case of dilute solution, where k_B is the Boltzmann constant, T is the ambient temperature, and S is the degree of supersaturation.

In our experiment, a levitated solution droplet increases its concentration by continuous water evaporation, which in turn, enhances the probability of crystal nucleation once it exceeds the solubility limit. For the nucleation to occur at any concentrations, at least one nucleus with the critical radius r^* is essential. This obvious assumption gives the relation,

$$\int_0^\tau I^s(\mathrm{S})V(\mathrm{S})dt = \sum_{t=0}^{t=\tau} I^s(\mathrm{S}) \times V(\mathrm{S}) \times t \geq 1 \ (1),$$

where I^s is the steady-state nucleation rate, V is a droplet volume, and t is time from $S = 1$ ($t = 0$) to onset of nucleation ($t = \tau$). Here, I^s per unit volume at T is given by,

$$I^s = \frac{6(n^*)^{2/3} k_B T N_A}{\pi \eta(C) a^3} \sqrt{\frac{\Delta\mu}{6\pi k_B T n^*}} exp\ (-\frac{\Delta G^*}{k_B \mathrm{T}}) \ (2),$$

with the average number of solutes in the nucleus $n^* = 32\pi v_m^2 \sigma^3/(3(k_B \mathrm{TlnS})^3)$, Avogadro's number N_A, viscosity of NaCl solution $\eta(\mathrm{C})$ as a function of concentration C, the average jump distance a, and the nucleation barrier $\Delta G^* = (4\pi/3)\sigma(r^*)^2$ where $r^* = 2\sigma v_m/k_B \mathrm{TlnS}$. $\eta(\mathrm{C})$ of the solution at high salt concentrations are obtained by data extrapolation for dilute solution.[10] Here, we use the unit cell length of NaCl crystal (564.02 pm) for a and the solid NaCl molar volume (27.06 cm^3) for v_m.

References

[1] D. R. Lide in *CRC Handbook of Chemistry and Physics*, (Eds: J. R. Rumble), CRC Press, **2005**.
[2] H. Yoo, C. Park, S. Jeon, G. W. Lee, *Metrologia* **2015**, *52*, 677-684.
[3] S. Lee, H. S. Wi, W. Jo, Y. C. Cho, H. H. Lee, S.-Y. Jeong, Y.-I. Kim, G. W. Lee, *Proc. Natl. Acad. Sci.* **2016**, *113*, 13618-13623.
[4] S. Lee, W. Jo, Y. C. Cho, H. H. Lee, G. W. Lee, *Rev. Sci. Instrum.* **2017**, *88*, 055101.
[5] D. Zahn, *Phys. Rev. Lett*. **2004**, *92*, 040801.
[6] S. Plimpton, *J. Comp. Phys*. **1995**, *117*, 1-19.
[7] I. S. Joung, T. E. Cheatham, *J. Phys. Chem. B* **2009**, *113*, 13279-13290.
[8] Q. Sun, *Vib. Spec.* **2009**, *51*, 213-217.
[9] Q. Sun, *Chem. Phys. Lett.* **2013**, *568*, 90-94.
[10] H.-L. Zhang, S.-J. Han, *J. Chem. Eng. Data* **1996**, *41*, 516-520.